Proceedings World Geothermal Congress 2020+1
Reykjavik, Iceland, April - October 2021

Fracture and Fault Analyses Based on Formation MicroImager Logs in the Lower Carboniferous of Two Geothermal Boreholes in Northern Belgium

Eva van der Voet[1,2,*], Ben Laenen[2], David Lagrou[2], Philippe Muchez[1] and Rudy Swennen[1]

[1] KU Leuven, Department of Earth and Environmental Sciences, Geo-institute, Celestijnenlaan 200E, B-3001 Leuven-Heverlee, Belgium

[2] Vlaamse Instelling voor Technologisch Onderzoek (VITO), Boeretang 200, B-2400, Mol, Belgium

[*] corresponding author: eva.vandervoet@kuleuven.be and eva.vandervoet@vito.be

Keywords: fractures, cusp, bed thickness, carbonates, Campine-Brabant Basin

ABSTRACT

Since the primary porosity of the Lower Carboniferous carbonates in the Campine-Brabant Basin is generally very low, fractures present in these rocks are of major importance for the permeability of this geothermal reservoir. A Formation MicroImager (FMI) geophysical well log is available from the first and third geothermal MOL-GT borehole drilled in Mol, northern Belgium. The FMI logs were used to identify different features based on resistivity contrasts, among which were bed boundaries and conductive fractures. These quantitative results enabled analysis of which factors control fracture characteristics and in which way. In one of the boreholes, thicker beds show larger mean fracture frequencies than thinner beds, while no such trend was found in the other borehole. Besides fractures, also possible fault intersections were interpreted from the FMI log of MOL-GT-03, based on changes in bedding dip and azimuth.

1. INTRODUCTION

The Lower Carboniferous carbonates in northern Belgium and the southern Netherlands are being used as a geothermal reservoir for a few years now (Broothaers et al., this volume). These fractured limestones and dolostones were deposited on a shallow water carbonate ramp to shelf in the so-called Campine-Brabant Basin. The carbonates generally contain a low primary porosity (in the order of a few percent), meaning that fractures have a major control on the permeability of the reservoir (Van der Voet et al., 2019). Therefore, understanding of the factors controlling fracture characteristics is needed in order to reduce the risks for future geothermal developments in the Campine-Brabant Basin.

The most direct approach to study fractures in these rocks is from borehole core material. Although joints might be difficult to quantify, because a discontinuity between two core samples could also be induced by drilling or handling the cores, partially open veins could be quantified. Van der Voet et al. (2020a) used the borehole of Heibaart DZH1, located in northern Belgium (figure 1), to study relationships between quantified fracture characteristics from cores and many other variables regarding lithology, geochemistry and geophysical well logs. This borehole was selected because of the large amount of (almost continuous) core material, the presence of different lithologies, the presence of open karstic features and the availability of multiple geophysical well logs. The authors found that fracturing in this sequence was controlled by differential compaction. Massive boundstones were fractured more intensely than layered wacke- to grainstones.

A Formation MicroImager (FMI) log is available from two of the three recently drilled boreholes in Mol, northern Belgium (Van der Voet et al., 2020b; figure 1). These MOL-GT geothermal wells were drilled from 2015 to 2018 for exploration of the Lower Carboniferous carbonate reservoir and for heat and power production (Bos & Laenen, 2017; Broothaers et al., this volume). An FMI log is an image log based on resistivity contrasts, on which bedding planes, fractures and possibly stylolites and faults are visible. In the cases of the MOL-GT-01 and MOL-GT-03 boreholes, these features were quantified from the FMI log and used to analyze factors influencing fracture characteristics. Results of the analyses of the MOL-GT-01 borehole were discussed by Van der Voet et al. (2020b). This first borehole was drilled vertical, while the third borehole was deviated towards the southeast with an inclination varying between 12 and 45 degrees in the Lower Carboniferous. Therefore, a comparison between the results of the first and third well could provide information about lateral variations of variables. Besides, the third borehole transects the entire Lower Carboniferous, down to a depth of 4238m (TVD). In this paper, the first results of the FMI analyses of MOL-GT-03 will be discussed, as well as a comparison with MOL-GT-01.

Besides the analyses of fracture characteristics, also possible faults were identified based on the FMI log. Increased fracture frequencies often occur around faults (Faulkner et al., 2010; Peacock et al., 2017), which is called a damage zone. These damage zones could be interesting from a geothermal perspective. In order to better understand the structural setting around the MOL-GT boreholes, possible fault intersections in MOL-GT-03 were interpreted and described in this paper.

2. GEOLOGICAL SETTING

The MOL-GT boreholes are located in Mol, northern Belgium (figure 1). During the Lower Carboniferous, a shallow sea was present in the Campine-Brabant Basin. On the northern edge of the London-Brabant Massif, carbonates were deposited on a ramp which evolved to a shelf during the Viséan (Reijmer et al., 2017). The carbonates were deposited on top of Devonian siliciclastics, mainly sandstones, and are overlain by Namurian shales.

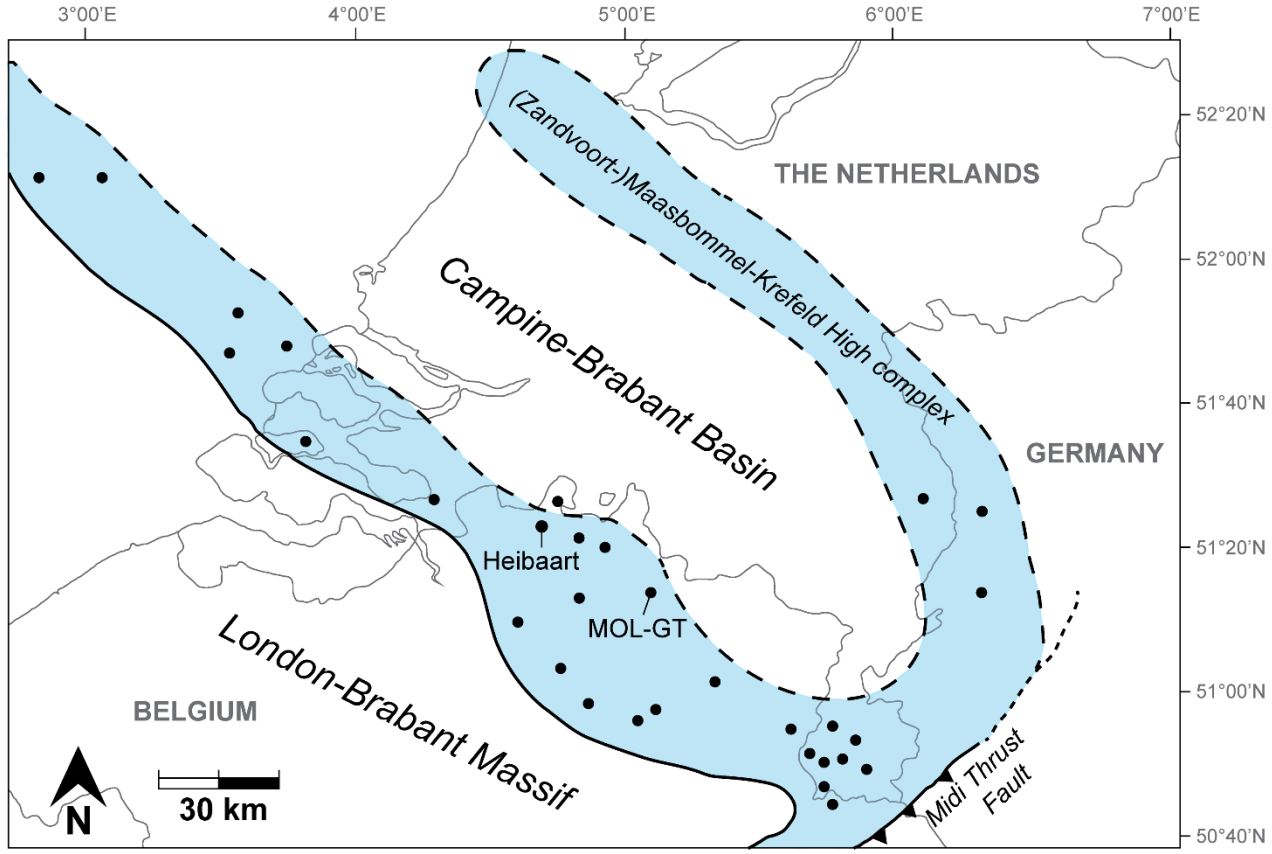

Figure 1: Location of the Campine-Brabant Basin, northeast of the London-Brabant Massif. The blue areas are the possible outlines of the carbonate ramp/shelf and the black dots are the locations of boreholes that were drilled into the Lower Carboniferous. Modified after Van der Voet et al. (2020a). At Heibaart, multiple boreholes were drilled by Distrigaz (Fluxys) in the context of an underground gas storage facility, of which DZH1 is one.

In MOL-GT-01, the Lower Carboniferous was intersected between 3175.5 m and 3610 m TVD, which is the total depth of the borehole (Bos & Laenen, 2017). The lower sequence, up to 3227.5 m, is part of the Loenhout Formation and consists of shallow water limestone with minor intercalations of shale and argillaceous limestone and one interval of dolostone around 3510 m (Van der Voet et al., 2020b). The upper part of the sequence comprises the Goeree Formation, which is an alternation of limestone and shale, and a small interval described as marl.

The Lower Carboniferous sequence of MOL-GT-03 is present between 3142 and 4010 m TVDBGL (3643-4673 m MDBGL) and comprises the Pont d'Arcole Formation between 3992 and 4010 m TVD, overlain by the Vesdre Formation between 3911 and 3992 m, the Steentje-Turnhout Formation between 3825 and 3911 m, the Velp formation between 3651 and 3825 m, the Loenhout Formation between 3192 and 3651 m, and the Goeree Formation between 3142 and 3192 m. The Goeree Formation consists of limestone interbedded with claystone. The Loenhout, Velp and Steentje-Turnhout Formations consists of limestone, with minor intercalations of claystone. Also, chert was found between 3210 and 3225 m. The Vesder Formation also contains mainly limestone and two intervals of dolostone between 3920 and 3970 m TVD. The Pont d'Arcole Formation comprises mainly claystone with minor intercalations of limestone.

The Lower Carboniferous in the Campine-Brabant Basin in northern Belgium was affected by synsedimentary (N)NW-(S)SE striking normal faults which created fault blocks and thickness differences of the sequence (Muchez & Langenaeker, 1993; Langenaeker, 2000). Both MOL-GT-01 and MOL-GT-03 were drilled as production wells and were aimed at the same fault zone in the Lower Carboniferous (Broothaers et al., this volume). From the FMI log of the first well, one clear 'cusp' was identified at a depth of 3284 m, which is a distinct increase and decrease of structural dip (Van der Voet et al., 2020b). It is interpreted to result from fault-tip folding and possibly the fault propagated through the folded layers. Besides, seven other possible but less clear fault intersections were identified in the Lower Carboniferous interval of this borehole.

3. METHODOLOGY

The interpretation of features from the FMI log of both boreholes was performed by Schlumberger geologists. The following features could be visually identified: bed boundaries, conductive fractures, drilling-induced tensile fractures, resistive fractures and stylolites. Bed boundaries appear as planar features which are darker than the matrix (more conductive). Since these are planes, they are visible on the enrolled FMI log as sinusoids. Conductive fractures are mostly steeper dipping planar features which are interpreted to be natural fractures filled with conductive material, which could be either clay minerals, mud or saline water. Drilling-induced tensile fractures are features which are visible as two lines with 180° of azimuth in between (opposite sides of the borehole), and are interpreted to be caused by the drilling of the borehole. Resistive fractures are fractures with a lower conductivity than the matrix,

interpreted as veins filled with cement. These resistive fractures are rarely visible since the resistivity contrasts with the matrix is rather small. Stylolites appear on the FMI log as mostly bedding-parallel planes with a serrated pattern.

Of every picked feature, the midpoint depth, azimuth and inclination were determined. In MOL-GT-01, the mean 'true bed thickness' was calculated by correcting the apparent bed thickness (along hole) for borehole inclination and subsequently for bed inclination (Van der Voet et al., 2020b). This borehole was drilled almost vertically. MOL-GT-03 was drilled much more deviated. Therefore, a more complex correction should be applied on the apparent bed thickness. Figure 2 shows the calculation of the true stratigraphic thickness (TST) from the measured thickness (MT) along hole, resulting in the equation of Tearpock & Bischke (1991). In this calculation, the azimuths of the borehole and the beds were taken into account as well.

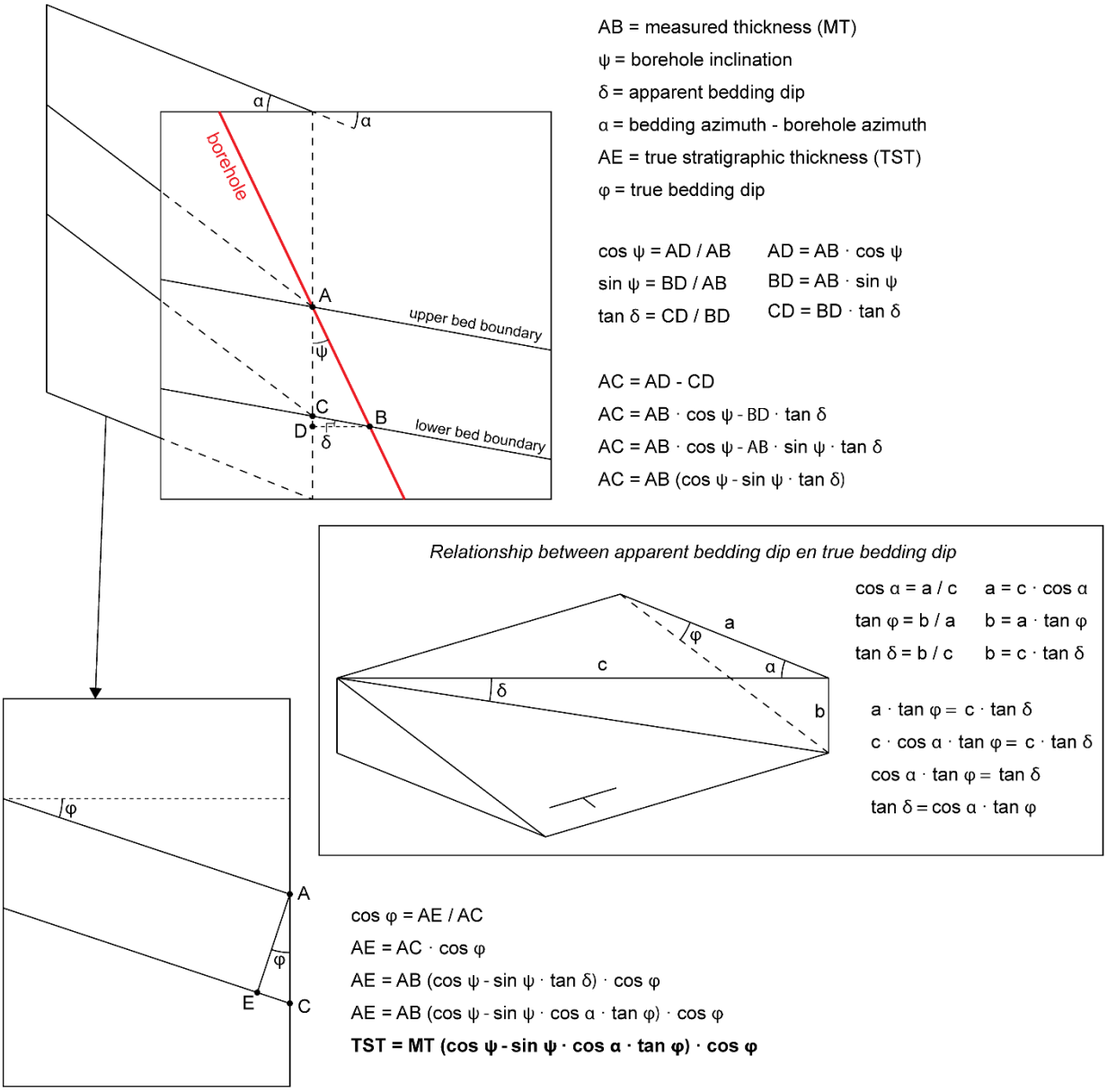

Figure 2: Calculation of the true stratigraphic thickness (TST) of a bed, from the measured thickness (MT) along hole.

In order to study the relationship between bed thickness and fracture frequency, the fracture numbers per bed should be corrected for orientation bias. Fractures with a normal parallel to the borehole are more likely to be transected by the borehole than fractures with a normal almost perpendicular to the borehole. To correct for this bias, a weighting factor (w) is assigned to each fracture (Terzaghi, 1965). The calculation of this weighting factor is explained in figure 3. To calculate the angle between the borehole and the fracture plane, the fracture's apparent dip (δ) in the borehole azimuth plane is calculated from the fracture's true dip (φ). Using the angle (β) between the borehole dip and the apparent fracture dip, the weighting factor is calculated by 1 / sin (β). This would mean that a fracture with a β of 90° is counted as 1, while a fracture with a β of 0° is counted as infinite. Multiple methods were proposed to account for the latter overestimation, but assumptions were made in these methods which are not applicable in this study. As an alternative widely used in literature, an arbitratry cut-off β of minimum 10° was used in this paper. So, the maximum weighting factor is 1/sin(10°). The resulting corrected fracture numbers were used to study the relationship between bed thickness and fracture frequency.

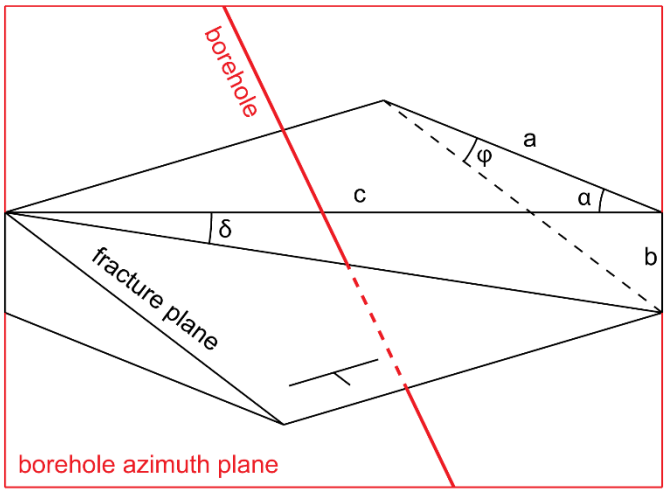

ψ = borehole inclination
δ = apparent fracture dip
α = fracture azimuth - borehole azimuth
φ = true fracture dip
β = angle between borehole dip and apparent fracture dip
F = fracture
w = weighting factor

$\tan \delta = \cos \alpha \cdot \tan \varphi$ (see figure 2)

$\delta = | \tan^{-1} (\cos \alpha \cdot \tan \varphi) |$

if cos α > 0 (apparent fracture dip in the borehole azimuth plane is in the same direction as the borehole)

if δ > 90 - ψ

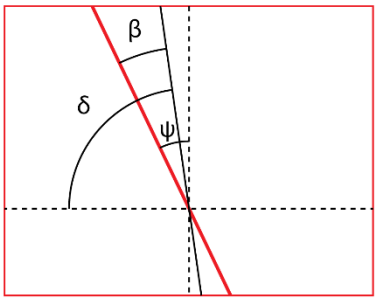

β = δ - (90 - ψ)

if δ < 90 - ψ

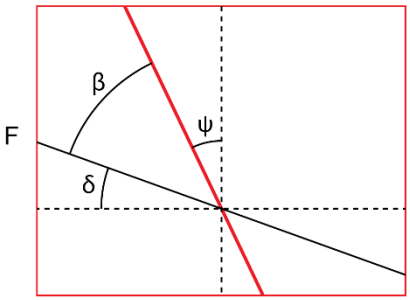

β = (90 - ψ) - δ

β = | (90 - ψ) - δ |

if cos α < 0 (apparent fracture dip in the borehole azimuth plane is in the opposite direction of the borehole)

if δ > ψ

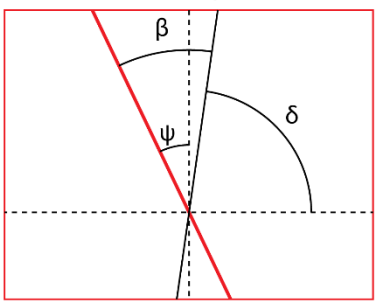

β = (90 - δ) + ψ

if δ < ψ

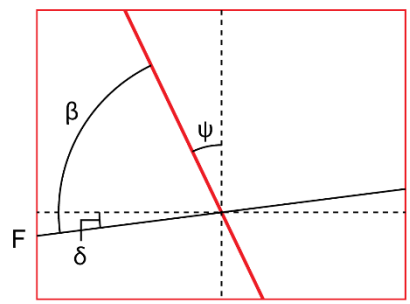

β = (90 - ψ) + δ

w = 1 / sin β

with β = minimum 10°

Figure 3: Calculation of the weighting factor, assigned to each fracture, to correct for orientation bias.

Furthermore, cusps were identified based on the FMI data. Criteria were a sudden increase and decrease of bedding inclination and/or a sudden change of bedding azimuth. We used a dip change of minimum 30° or an azimuth change of at least 90°. A sharp increase and decrease of bedding inclination with depth could indicate fault-tip folding (Etchecopar & Bonnetain, 1992; Hesthammer & Fossen, 1998; Van der Voet et al., 2020b). A change in azimuth could be caused by a fault, a fold or an unconformity. For every possible fault intersection, the visibility of the bedding planes on the FMI log was checked. If bedding planes are well visible, the certainty of interpreting a fault is larger than if bedding planes are not well visible. Drilling parameters were checked for possible fault indications. Based on the combination of all these criteria, a relative confidence level was assigned to every possible fault.

4. RESULTS

4.1 Bed thickness and fracture frequency

The mean true stratigraphic bed thickness (TST) in MOL-GT-03 is 11 cm. No bed boundaries could be picked in a zone around 4350 m (MD) where the quality of the FMI log is lower than in the rest of the Lower Carboniferous. The TST was also calculated for MOL-GT-01, resulting in a mean TST of 9 cm. In order to emphasize the variation, the logarithm of these true stratigraphic bed thicknesses is plotted along the depth of both boreholes in figure 4. The bed thickness in the first borehole is rather constant, except the sequence between 3220 m and 3310 m in which beds are thicker. In both boreholes, bed thickness increases downwards within the Goeree Formation. MOL-GT-03 shows more variation in bed thickness. Thin beds occur in the zones 4070-4140 m and 4430-4560 m. Relatively thick beds are mainly present in the zone 3720-3760 m. Rapid changes occur around 4600 m depth.

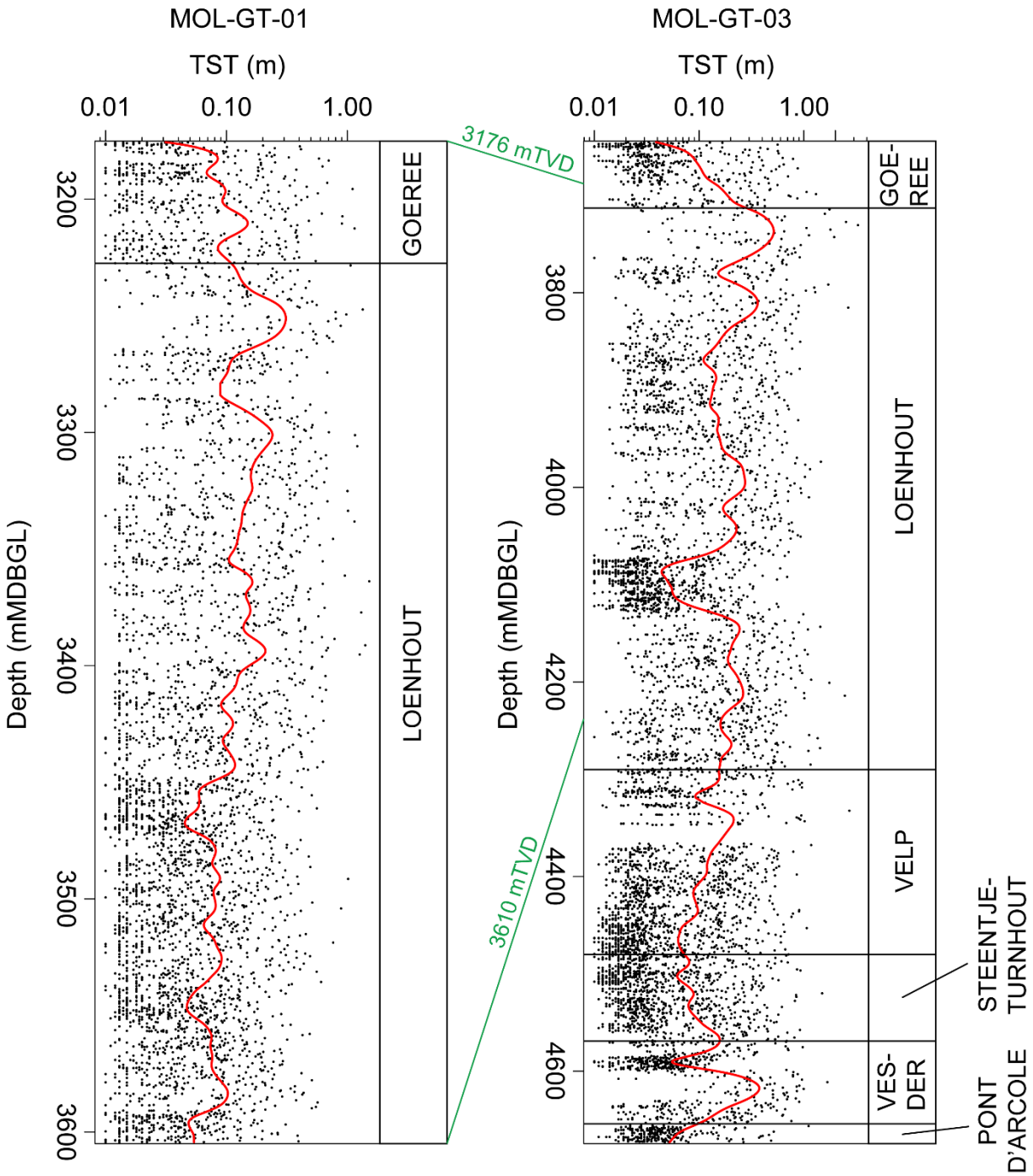

Figure 4: True stratigraphic thickness (TST) of beds in both boreholes. The red lines represent smoothing splines of the TST values.

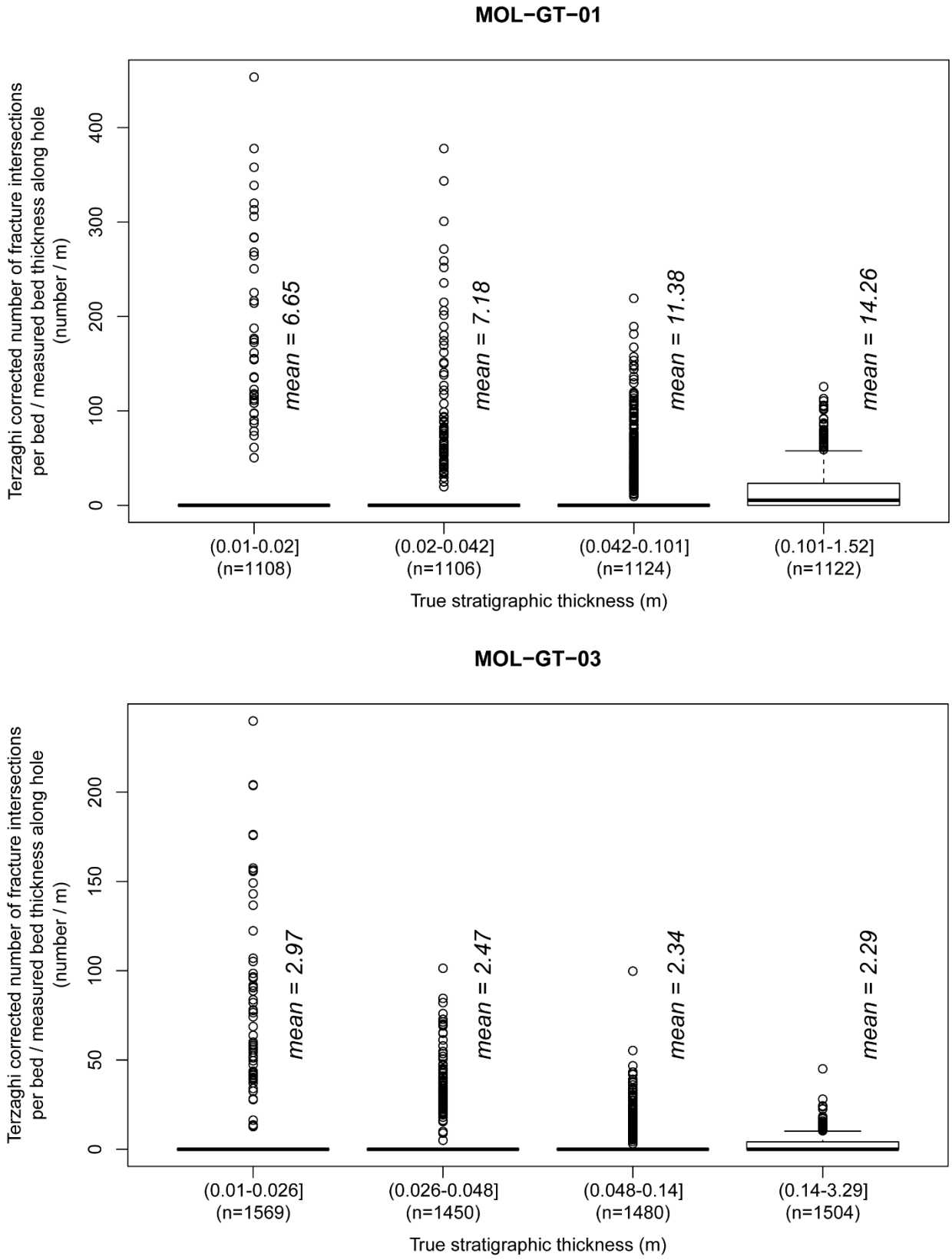

Figure 5: Boxplots showing the 'fracture frequency' (Terzaghi corrected number of fracture intersections per bed, divided by the measured bed thickness along hole) for 4 almost equally sized groups of true stratigraphic bed thickness. The upper plot shows the results of MOL-GT-01 and the lower one of MOL-GT-03. Note that many beds contain 0 fracture intersections. The mean fracture frequency of each TST group is shown as well.

Figure 5 shows the TST of the beds on the x-axis, subdivided into four groups of almost equal bed numbers. Only beds with a TST of minimum 1 cm were taken into account. For each bed, the Terzaghi corrected number of fracture intersections was divided by the measured bed thickness, because the longer the borehole transect within the bed, the more fractures could be intersected. This 'fracture

frequency' is clearly higher in MOL-GT-01 (on average 9.77 m^{-1}) than in MOL-GT-03 (on average 2.58 m^{-1}). The 'fracture frequency' is plotted on the y-axis of figure 5. Because of the large number of beds with 0 fracture intersections, the boxplots are mostly only visible as lines on the bottom of the plot, with exceptions of beds with larger fracture frequency visible as circles above it. For each TST category, the mean fracture frequency is shown in figure 5 as well. It is hardly visible because of the many beds without fractures, but the mean fracture frequency in MOL-GT-01 increases from 6.65 fractures per meter in the beds of 1 to 2 cm, to 14.26 fractures per meter in the beds thicker than 10.1 cm. This means that thicker beds on average contain higher fracture frequencies than thinner beds. In MOL-GT-03, the mean fracture frequency decreases from 2.97 fractures per meter in beds of 1 to 2.6 cm, to 2.29 fractures per meter in beds thicker than 14 cm. This difference is very small, in general the mean fracture frequency is comparable for all bed thicknesses.

4.2 Possible fault interpretations

Based on changes in bedding inclination and azimuth, seven possible fault intersections were determined in MOL-GT-03. In figure 6, the inclination and azimuth of bed boundaries are plotted along depth (MD). The arrows indicate the depths of the possible fault intersections, at which sudden bedding inclination and/or azimuth changes are present. Table 1 summarizes the analyzed criteria for each possible fault. Besides changes in bedding inclination and azimuth, also the depth uncertainty is mentioned and the visibility of bed boundaries on the FMI log. Other characteristics of the possible fault zones were described. Based on the magnitude of the changes in bedding inclination and azimuth, as well as the visibility of bed boundaries and anomalies in drilling parameters, a relative confidence level was assigned to each possible fault intersection. The cusp at 4352 m depth was assigned a confidence level of 1, which means the highest certainty of the presence of a fault (green arrow in figure 6). Level 4 means the lowest certainty (red arrows).

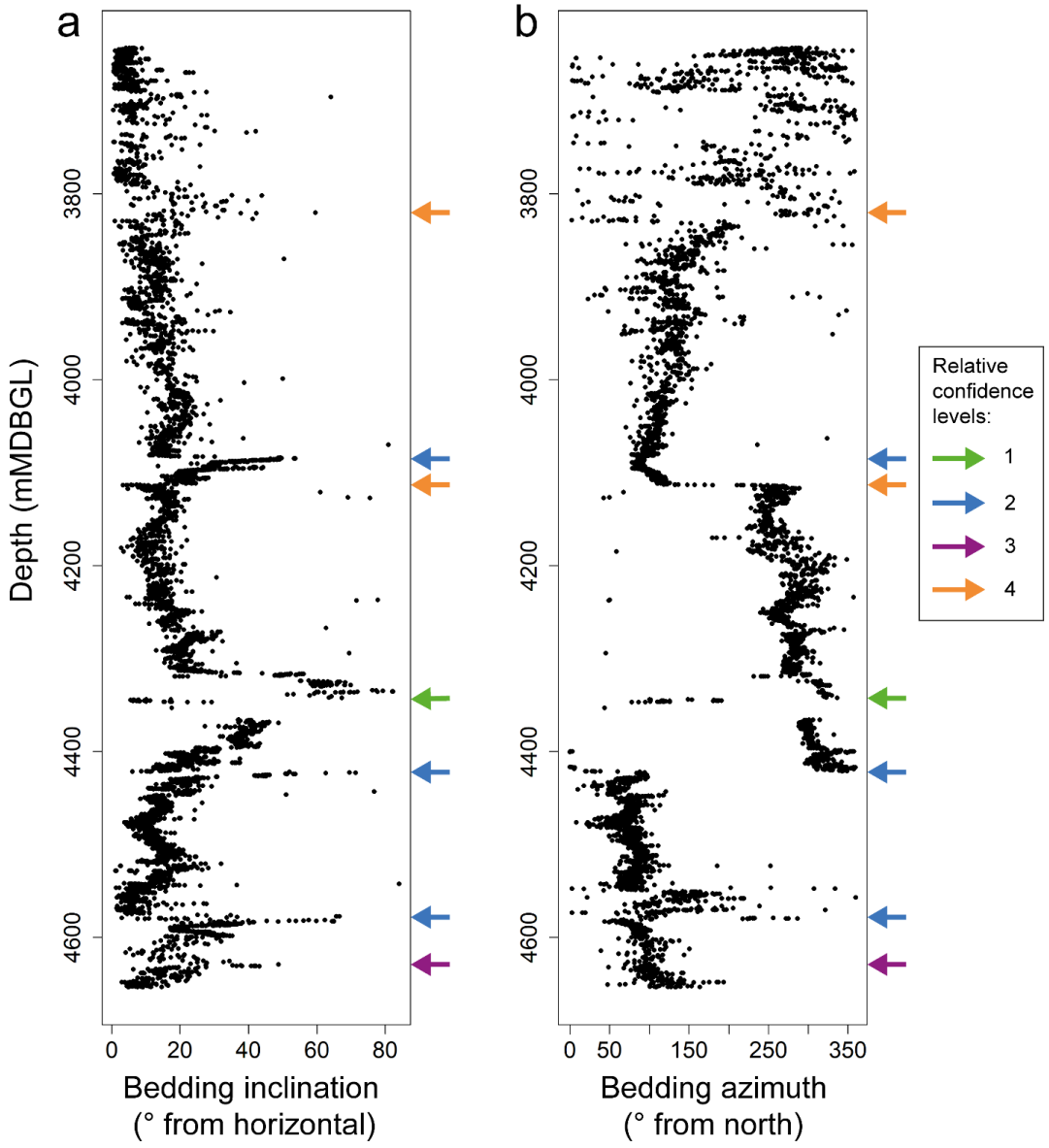

Figure 6: Inclination (a) and azimuth (b) of bed boundaries along the depth (MDBGL) of MOL-GT-03. The depths of the interpreted possible fault intersections are indicated by the arrows on the right, of which the color refers to the relative confidence level (1 being most confident).

Table 1: Description of various aspects of the interpreted possible fault intersections in the Lower Carboniferous of MOL-GT-03

Depth (mMD BGL)	Depth (mTVD BGL)	Dip change	Azimuth change (dip direction)	Bed boundaries well visible	Descriptions	Other fault indications	Relative confidence level
3820 +/- 5	3270	Dip varying between 3790 and 3830 m (1-60°). Gradual increases and decreases around peaks at 3801.8 m (44°), 3807.4 m (40°), 3820.3 m (60°) and 3826.9 m (41°).	Azimuth varying over 360° in this interval. Sudden change from N266E at 3823.4 m to N106E at 3823.8 m and N002E at 3828.4 m. Downward gradually changing to eastern and southern direction (3835 m).	Medium	Varying dip but gradually increasing and decreasing between 3790 m and 3830 m with strongly varying azimuth. No fault plane visible.		4
4085 +/- 0.5	3477	From 4082.5 to 4084.7 m: steepening from 20° to 54°. From 4084.7 to 4112.9 gradual dip decrease to 14°, with exception of peak at 4094.2 m (44°).	No azimuth change.	Yes	Sharp dip increase and gradual decrease, with second smaller peak, considered as one structure. No fault plane visible.		2
4113 +/- 0.5	3500	Dip decrease from 14° at 4112.9 m to 8° at 4113.1 m. Further decrease to 3° at 4113.6 m.	Changing from ca. N117E and N262E between 4112 and 4114 m.	Yes	Slightly decreasing dip and sharp azimuth change. No fault plane visible.		4
4343 +/- 20	3699	From 4310.0 to 4316.5 m: steepening from 19° to 56°. Dip decrease to 18° between 4318.3 and 4319.2 m. Rather stable dip between 4323.8 and 4342.3 m. Between 4342.3 and 4343.9: drop from 67° to 10°. Gradual increase from 4344.6 to 4346.9 m: 6° to 29°. Only 1 bedding plane visible between 4346.9 and 4366.0 m.	No large change on the large scale (ca. N270E to N320E), but a few beds have azimuths to N231E (4319.2 m), and between N043E and N191E in the zone 4343.9-4353.2 m.	No	Zone with very few interpreted bed boundaries and 4 stylolites. Downward increasing dip, with sudden drop at 4343 m. No fault plane visible.	Caliper variations in this interval	1
4422 +/- 1	3771	Very gradual dip decrease between 4369.3 and 4420.9 m: 49° to 14°. Steeper dip decrease from 4420.9 to 4421.5 m: 14° to 6°. Sudden steepening downward to 71° at 4422.8 m. Gradual dip decrease to 20° at ca. 4430 m.	Azimuth change from N343E at 4421.1 m to N020E at 4421.3 m, to N094E at 4422.7 m.	Yes	Gradual dip decrease with sudden steepening at 4421.5 m. Possible fault plane visible at 4422.8 m.		2

4578 +/- 3	3920	Between 4574.8 and 4577.5 m: steepening from 5° to 67°. Dip decrease downward to 3° at 4579.1 m and increase again to 65° at 4582.7 m.	Azimuth varies largely in overlying strata. Gradual change from N099E at 4575.8 m to N044E at 4582.9 m, except beds with an azimuth of N217E-N287E between 4579.1 and 4580.1 m.	No	Bedding dip increase and strongly varying azimuth. Many interpreted stylolites in this zone. No fault plane visible.	Positive caliper anomaly	2
4629 +/- 2	3968	Gradual dip increase between 4616.2 to 4629.2 m: from 4° to 49°. Gradual dip decrease downward to 3° at 4648.1 m.	No azimuth change.	Medium	Gradual dip increase and decrease. Many interpreted stylolites between 4599 m and 4631 m. No fault plane visible.	Positive caliper anomaly	3

5. DISCUSSION

Van der Voet et al. (2020b) found that relatively thin beds contain relatively many conductive fractures, and vice versa, in the borehole MOL-GT-01. These authors used a comparison with a hypothetical situation of evenly distributed fractures. The present study analyzed the relationship between bed thickness and fracture frequency for both boreholes in a different way, using the true stratigraphic thickness and mean frequencies of bed thickness groups. No clear correlation between bed thickness and fracture frequency is present, but the mean fracture frequency is larger in thicker beds than in thinner beds in MOL-GT-01. This differs from the conclusion of Van der Voet et al. (2020b) because of improved corrections and a different method of normalization, which was necessary in MOL-GT-03 because of its deviated well path. In MOL-GT-03, fracture frequencies are rather similar for different bed thickness groups. A relationship between fracture frequency and bed thickness has often been described in literature (Bogdonov, 1947; Price, 1966; Hobbs; 1967; Sowers; 1972; Narr & Suppe, 1991; Gross, 1993). However, most of the authors found that fracture frequency *decreases* with increasing bed thickness. In the case of the MOL-GT boreholes, the relationship is not obvious (since the variation is large) but in MOL-GT-01, an opposite trend is visible. In general, the influence of bed thickness on fracture frequency appears to be limited.

Besides fractures, also faults could have a large influence on the permeability in a geothermal reservoir. In MOL-GT-03, the fault intersection which was interpreted with the largest certainty, is located at a depth between 4323 and 4363 m MD, which is 3707 m TVD. This is deeper than the total depth of MOL-GT-01. The most obvious cusp in MOL-GT-01 is present at a depth of 3284 m TVD. So, several possible fault intersection were identified in both wells. However, no conclusions can be drawn at this stage on the possible continuation of faults between both boreholes.

6. CONCLUSIONS

In Van der Voet et al. (2020b), the FMI log of the MOL-GT-01 borehole was used to check which factors control fracture characteristics. The influence of bed thickness, possible fault intersections and lithology was tested. In this paper, these results were compared to the results of the MOL-GT-03 borehole. The effect of bed thickness on fracture frequency was analyzed and no clear relationship was found. In MOL-GT-01, thicker beds contain relatively high fracture frequencies, while thinner beds contain relatively low frequencies. This trend was not visible in MOL-GT-03. Furthermore, seven possible fault intersections were interpreted in MOL-GT-03, of which the one at 4352 m MD has the largest certainty.

ACKNOWLEDGEMENTS

The research is supported by a VITO PhD grant nr. 1610424.

REFERENCES

Bogdonov, A.A.: The intensity of cleavage as related to the thickness of beds. *Soviet Geology,* **16**, (1947).

Bos, S., and Laenen, B.: Development of the first deep geothermal doublet in the Campine Basin of Belgium, *European Geologist*, **43**, (2017), 16-20.

Broothaers, M., Bos, S., Lagrou, D., Harcouët-Menou, V., and Laenen, B.: Insights into a complex geothermal reservoir in the Lower Carboniferous carbonates in northern Belgium, World Geothermal Congress 2020, Reykjavik, Iceland, April 26 – May 2, 2020.

Etchecopar, A., and Bonnetain, J.L.: Cross sections from dipmeter data, *AAPG Bulletin*, **76**, (1992), 621-637.

Faulkner, D.R., Jackson, C.A.L., Lunn, R.J., Schlische, R.W., Shipton, Z.K., Wibberley, C.A.J., and Withjack, M.O.: A review of recent developments concerning the structure, mechanics and fluid flow properties of fault zones, *Journal of Structural Geology*, **32**, (2010), 1557-1575.

Gross, M.R.: The origin and spacing of cross joints: examples from Monterey Formation, Santa Barbara Coastline, California. *Journal of Structural Geology*, **15**, (1993), 737–751.

Hesthammer, J., and Fossen, H.: The use of dipmeter data to contstrain the structural geology of the Gullfaks Field, northern North Sea, *Marine and Petroleum Geology*, **15**, (1998), 549-573.

Hobbs, D.W.: The formation of tension joints in sedimentary rocks: an explanation. *Geological Magazine*, **104**, (1967), 550-556.

Laenen, B., Van Tongeren, P., Dreesen, R., and Dusar, M.: Carbon dioxide sequestration in the Campine Basin and adjacent Roer Valley Graben (North Belgium): an inventory, *Geological Society, London, Special Publications*, **233**, (2004), 193-210.

Langenaeker, V.: The Campine Basin: stratigraphy, structural geology, coalification and hydrocarbon potential of the Devonian to Jurassic, *Aardkundige Mededelingen*, **10**, (2000), 1-142.

Muchez, P., and Langenaeker, V.: Middle Devonian to Dinantian sedimentation in the Campine Basin (Northern Belgium): its relation to Variscan tectonism, *Special publications of the International Association of Sedimentologists*, **20**, (1993), 171-181.

Narr, N. & Suppe, J.: Joint spacing in sedimentary rocks. *Journal of Structural Geology*, **13**, (1991), 1037–1048.

Peacock, D.C.P., Dimmen, V., Rotevatn, A, and Sanderson, D.J.: A broader classification of damage zones, *Journal of Structural Geology*, **102**, (2017), 179-192.

Price, N.J.: Fault and Joint Development in Brittle and Semi-Brittle Rocks. Pergamon Press, Oxford, (1966).

Reijmer, J.J.G., Ten Veen, J.H., Jaarsma, B., and Boots, R.: Seismic stratigraphy of Dinantian carbonates in the southern Netherlands and northern Belgium, *Netherlands Journal of Geosciences*, **96**, (2017), 353-379.

Sowers, G.M.: Theory of spacing of extension fracture. *International Journal of Geoengineering Case Histories,* **9**, (1972), 27-53.

Tearpock, D.J., and Bischke, R.E.: Applied Surface Geological Mapping. PrenticeHall, Inc. Englewood Cliffs, New Jersey, (1991).

Terzaghi, R.D.: Sources of errors in joint surveys. *Geotechnique*, **15**, (1965), 287–304.

Van der Voet, E., Laenen, B., Lagrou, D., Muchez, P., Weltje, G.J. and Swennen, R.: Fracturing in Lower Carboniferous carbonates in the Campine-Brabant Basin (northern Belgium): borehole analyses, Proceedings of the European Geothermal Congress 2019, The Hague, The Netherlands, (2019), 1-5.

Van der Voet, E., Muchez, P., Laenen, B., Weltje, G.J., Lagrou, D., and Swennen, R.: Characterizing carbonate reservoir fracturing from borehole data – a case study of the Viséan in northern Belgium, *Marine and Petroleum Geology*, **111**, (2020a), 375-389.

Van der Voet, E., Laenen, B., Rombaut, B., and Swennen, R.: Fracture characteristics of Lower Carboniferous carbonates in northern Belgium based on FMI log analyses, *Netherlands Journal of Geosciences*, **99**, (2020b).